PIEZOELECTRIC MICRO POWER GENERATOR FOR ENERGY HARVESTING

R. Sood, Y.B. Jeon, J.-h. Jeong and S.G. Kim
Department of Mechanical Engineering, Massachusetts Institute of Technology
Cambridge, MA 02139

ABSTRACT

A thin film lead zirconate titanate $Pb(Zr,Ti)O_3$ (PZT), power generating device is developed. It is designed to resonate at specific vibrational frequencies from an ambient, vibrational energy source, thereby creating electrical energy via the piezoelectric effect. The energy harvesting device uses the piezoelectric d_{33} mode and is fabricated with three mask steps. Our cantilever device was designed to have a flat structure with a proof mass added to the end. A method for controlling the bowing curvature of the cantilever was applied by modulating the residual stress and elastic properties of the composite beam. The top electrode of Ti and Pt was patterned into an interdigitated shape on top of the sol-gel-spin coated PZT thin film in order to employ the d_{33} mode of the piezoelectric. This d_{33} mode design can generate at least a 20 times higher voltage than that of the d_{31} mode design. The device was mechanically excited by base shaking experiments, which revealed that our device has three resonance modes. The base-shaking experiments at the first resonant frequency (13.9 kHz) demonstrated that the generated charge is proportional to the tip displacement of the cantilever with an approximate linearity coefficient of 4.14 pC/μm. The total system can deliver 1μW of continuous electrical power to a 5.2MΩ resistive load at 2.4V DC. The corresponding energy density is 0.74 mW-h/cm^2, which compares favorably to current chemical batteries (i.e. lithium ion). We expect the optimized design to generate a much higher power level than we have now by targeting and harvesting from lower frequency vibrations.

INTRODUCTION

Energy harvesting from the environment has been actively explored using many methods such as solar power (most familiar ambient energy source), electromagnetic fields (used in RFID tags, inductively powered smart cards, etc.), thermal gradients, fluid flow, energy produced by the human body, and the action of gravitational fields [**1**]. Most of all, mechanical vibration is a potential power source which can be used for conversion to electrical energy through Microelectromechanical systems (MEMS) technology. Piezoelectric materials are perfect candidates for harvesting power from ambient vibration sources because they can efficiently convert mechanical strain to an electrical signal [**2,3**]. Several bulk piezoelectric generators have already been developed using the d_{31} piezoelectric mode [**1,4,5**], but there has been no d_{33} thin-film piezoelectric generators at the scale of MEMS. In this study, we describe a MEMS-based power scavenger employing the piezoelectric thin film with the d_{33} mode, named here as the Piezoelectric Micro Power Generator (PMPG).

DESIGN

The energy conversion from mechanical vibration into electrical power can be formulated as a general model given mathematically by Eq. (1) [**1,6**]:

$$m\ddot{z}_o + (b_e + b_m)\dot{z}_o + kz_o = -m\ddot{z}_i \tag{1}$$

where z_o is the device output (tip) displacement, z_i is the input (base) displacement, m the lumped mass, b_m the mechanical damping coefficient, b_e the electrically induced damping coefficient, and k the stiffness of the MEMS device.

The power converted to the electrical system is given by:

$$P = \frac{1}{2} b_e \dot{z}_o^{\,2} \tag{2}$$

PMPG devices should be designed so that they mechanically resonate at a frequency tuned to the ambient vibration source in order to generate maximum electrical power. The resonance frequency is approximately given as $\omega_n = \sqrt{k/m}$ by its stiffness (k), and mass (m). Thus, the devices could be tuned at different frequencies by varying the beam dimensions and/or mass of the moving parts (i.e. layer thicknesses and the inclusion of a proof mass, if necessary). Eqs. (1) and (2) provide us with the converted power at resonance [**1**]:

$$|P| = \alpha \omega^3 Y^2 = \alpha \frac{A^2}{\omega} \tag{3}$$

where $\alpha = \frac{m\zeta_e}{4\zeta_T^2}$, Y is the displacement magnitude of input vibrations, A is the acceleration magnitude, ζ_e and ζ_T the electrical and total damping ratios.

In order to get as much power as possible, we initially hypothesized that the device needed to be operated at a high frequency and have a high amplitude vibration source. However, it should be noted that the displacement amplitude decreases rapidly as the frequency goes up. We also found that most of the available environmental vibrations were at low frequencies and had high acceleration magnitudes. We will optimize the design in the next generation device fabrication.

A cantilever beam structure was chosen for the geometric design. There are two piezoelectric modes (d_{31} and d_{33}), which are commonly used in piezoelectric devices. Figure 1 is a cross-sectional view of these two device modes. They are distinguished by whether the electric field direction is perpendicular to the input strain direction (d_{31}) or parallel to it (d_{33}). Eqs. (4) and (5) show the relation between stress σ_{xx} (or strain x_3) and electric field E_i (or voltage V_{3i}).

$$x_3 = d_{3i} E_i \tag{4}$$

$$V_{3i} = \sigma_{xx} g_{3i} L_i \tag{5}$$

where x_3 is the strain, V_{3i} the open circuit voltage, d_{3i} (V/m) and g_{3i} (Vm/N) the piezoelectric constants, and L_i is the distance between electrodes which could be either t_{pzt} or L. The d_{3i} coefficient is directly proportional to g_{3i} via the dielectric coefficient (ε_{pzt}) of the piezoelectric.

While the d_{31} type must have separate top and bottom electrodes, the d_{33} type eliminates the need for a bottom electrode by employing an interdigitated (IDT) top electrode. This reduces the number of photo masks needed for a d_{33} piezoelectric device compared with the d_{31} device. In the d_{31} case, L_1 from Eq. (5) is limited to the thickness of the PZT layer t_{pzt}, while L_3 can be independently long (~10*t_{pzt}) in the d_{33} case. In addition, since the magnitude of the d_{33} and g_{33} coefficients are 2 to 2.5 times larger than their d_{31} and g_{31} counterparts, the generated, open-circuit

voltage of a d_{33} type device will be much larger (20 times or greater) than a d_{31} type transducer of similar beam dimensions. This then enables the activation of the rectifying circuit. In this regard, the d_{33} mode was employed to make our PZT micro cantilever device.

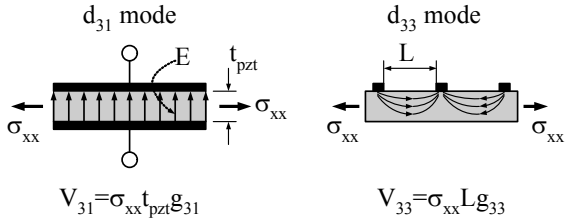

Figure 1. *Two modes of piezoelectric conversion from input mechanical stress.*

FABRICATION

A d_{33} mode, thin film, lead zirconate titanate (also known as PZT) cantilever device was fabricated using three photo masks. Figure 2 shows the device schematic of the d_{33} mode PMPG device. The alternating plus and minus potentials are imposed upon the mini-electrodes when the PZT is poled. The basic design of the multilayer structure consists of five layers as follows: membrane layer (SiO_2 and/or SiN_x) for controlling bow of the cantilever structure, diffusion barrier/buffer layer (ZrO_2) for preventing electrical charge diffusion from the piezoelectric layer, piezoelectric layer (PZT), top IDT electrode (Pt/Ti), and optional proof mass layer (SU-8).

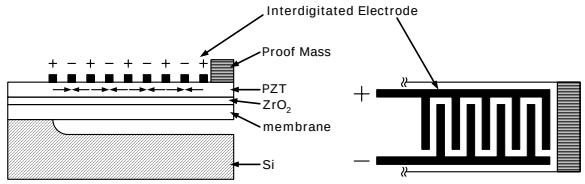

Figure 2. *Schematic of d_{33} mode piezoelectric device.*

First, the membrane layer is deposited on the Si wafer. In order to control the residual stress of the cantilever beams, several different kinds of membrane/buffer layer combinations were deposited such as 0.05μm ZrO_2/0.4μm thermal oxide, 0.05μm ZrO_2/0.4μm PECVD oxide, and 0.05μm ZrO_2/(0.1μm PECVD oxide/0.4μm SiN_x). Each PECVD oxide layer is annealed at 750°C for 30 minutes. The 50 nm thick ZrO_2 layer is deposited via a sol-gel spin-on process, then dried at 350°C for 1 minute, and annealed at 700°C for 15 minutes.

The PZT solution (Mitsubishi Materials Co.) has a composition of Pb/(Zr+Ti) of 118/100 along with a Zr/Ti ratio of 52/48. The solution is spun on the substrate at 500 rpm for 3 seconds and 1500 rpm for 30 seconds. The precursor gel film is pyrolyzed at 350°C for 5 minutes on a hot plate in several repeated cycles to create a PZT layer with 0.48μm thickness. The PZT film is then annealed at 700°C for 15 minutes. The PZT layer and membrane layers are patterned via RIE with BCl_3:Cl_2 (30:10) for 70 min with the first mask. The top IDT electrode is deposited next with 20 nm Ti and 200 nm Pt via e-beam evaporation and patterned using a lift-off procedure with the second mask. The SU-8 is spin-coated on top of the existing layers and patterned with the third mask to create the proof mass. A wet etching process such as KOH etch was initially used to release the cantilever structure, but it showed stiction problems and the KOH was found to attack the PZT layer. We solved this problem by employing an isotropic XeF_2 vapor etching which uses the PZT layer itself as the etch mask. This was possible because XeF_2 has a high etch selectivity between Si and the other layers. An SEM image of the fabricated PMPG device is shown in Figure 3.

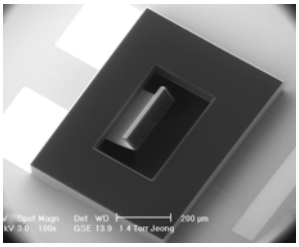

Figure 3. *SEM of the fabricated PMPG device with bond pads.*

The bow of the composite cantilever beam was controlled by changing its bottom layer from thermal SiO_2 to PECVD SiO_2, then to SiN_x. This approach was used for optimizing the residual stress and elastic modulus. On the basis of the data in Table 1, we have calculated the bow curvature as a function of residual stress and elastic modulus and determined that reducing the bow requires two parts: changing the residual stress of the bottom layer from compressive to tensile and increasing its elastic modulus.

Figure 4 shows that our strategy is appropriate. The first device, with thermal SiO_2 of about -300 MPa being the bottom layer, has a severely curled cantilever (Fig. 4(a)). In Fig. 4(b), this bow was greatly diminished by depositing SiO_2 via PECVD, by which the residual stress in the bottom layer is reduced to only tens of MPa. There is a trade off in choosing the elastic modulus. In the smaller elastic modulus regime, it is easier to control the curvature. However, even a small perturbation of the intended stress can result in a very large change of the final curvature. Selecting a large elastic modulus actually gives us more robustness in fabricating the device. For this reason, a SiN_x layer of high elastic modulus (313 GPa) and tensile stress (190 MPa) was selected as the bottom layer. A nearly flat cantilever beam was obtained as can be seen in Fig. 4(c).

Table 1. *Mechanical properties and residual stresses of films deposited for the cantilever structure. PZT number indicates the order in which the PZT film was deposited on top of the ZrO_2 layer. The stress was measured by a curvature method.*

	PZT1**[7]**	PZT 2	PZT3	PZT 4	ZrO_2 **[8]**	SiO_2 **[9]** (thermal)	SiO_2 **[9]** (PECVD)	SiN_x **[10]**
Elastic Modulus [GPa]	63	63	63	63	244	69	69	313
Poisson Ratio	0.30	0.30	0.30	0.30	0.27	0.15	0.15	0.29
Residual Stress [MPa]	630/610	-115/-125	75/65	113/105	400/350	-280/-330	35/-15	210/170

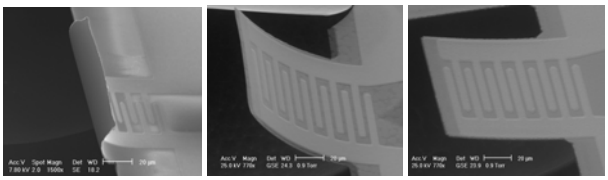

(a) (b) (c)

Figure 4. *SEM images of the stress-controlled cantilevers consisting of (a) PZT/ZrO_2/SiO_2(thermal), (b) PZT/ZrO_2/SiO_2(PECVD) and (c) PZT/ZrO_2/SiO_2(PECVD)/SiN_x.*

CHARACTERIZATION

The PMPG device acts as an AC current generator in parallel with a complex output impedance. While the PMPG is mechanically resonating ($z_o(t)$) at frequency ω_n, the PZT thin film experiences a time-varying change in mechanical stress ($\sigma(t)$), alternating from tensile to compressive. This results in a time-varying generated charge within the PZT layer, which is the source of the AC current. Taking the first time derivative of the charge function Q(t) gives the AC current source $I_P(t)$. A rectifying circuit and electrical storage capacitor are required for rectifying and storing the electrical energy for each device (Fig. 5).

The device chip was packaged on a multiple pinned ceramic package. Each device has two bond pads (Fig. 3), which are connected via wire bonding and soldering to the measurement electronics (charge amplifier) and proto board containing the external rectification circuitry, storage capacitor, and resistive load. The device was heated to 100 °C on a hot plate and poled at 90V DC for 30 minutes. The temperature was then cooled down to room temperature while maintaining the 90 V applied voltage.

The rectification bridge circuit consists of four STMicroelectronics® 1N5711 small signal Schottky diodes and a 10 nF mylar storage capacitor. These diodes were chosen specifically because, compared to most discrete components, they have the smallest forward voltage drop (approximately 0.2V). This allows for the largest possible DC voltage to develop across the capacitance/load. The 10 nF mylar cap was chosen because it has a very low leakage current.

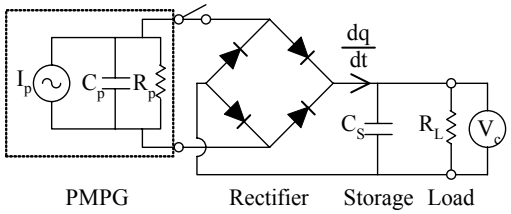

Figure 5. *Equivalent electrical model of the PMPG power system.*

RESULTS AND DISCUSSION

The polarization properties of the PZT thin films were measured using the Radiant Technologies© RT-66A High Voltage Interface with Trek® Model 601C in the form of a P-V hysteresis curve. The spontaneous polarization (P_s), remanent polarization (P_r), coercive field, and dielectric constant are 50 μC/cm^2, 20 μC/cm^2, 38 kV/cm, and 1200ε_0, respectively.

In order to find out the resonance mode and tip displacement, the PMPG device of 170 μm×260 μm was directly excited by a ±3V AC voltage source and swept from 0 to 200 kHz. At the same time, the cantilever tip displacement was measured by a laser vibrometer. Figure 6 reveals three resonant modes: 13.9, 21.9 and 48.5 kHz. The 13.9 kHz mode is the uniform bending mode of concern, and also demonstrates the largest tip displacement amplitude. The 48.5 kHz is also a bending mode, but the beam bends both upward and downward in a snake-like fashion, while the 21.9 kHz mode demonstrates a twisting type motion (torsional mode). Since the 13.9 kHz 1st resonance mode shows the largest amplitude of displacement, we can obtain the highest power output from it.

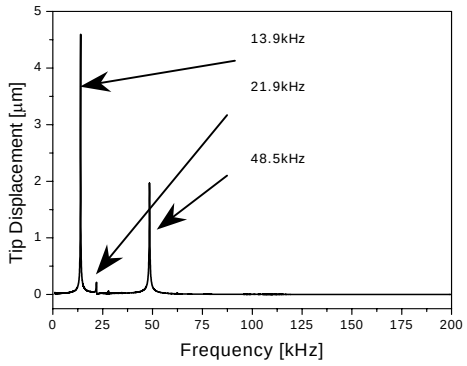

Figure 6. *Cantilever tip displacement vs. AC frequency.*

Having determined the 13.9 kHz 1st mode resonance, a piezoelectric shaker was then used to apply vibration directly to the PMPG at that frequency. The magnitude of the base displacement was varied by changing the shaker drive voltage amplitude. Cantilever tip displacement and the corresponding closed-circuit charge (measured by a closed-circuit charge amplifier) were then measured against the input base displacement (Fig. 7). Here, base displacement is simply the displacement of the silicon substrate to which the micro cantilever is attached. The tip displacement was amplified by approximately 90 times over the base displacement during resonance. On the whole, tip displacement was linear to base displacement except during large base displacements.

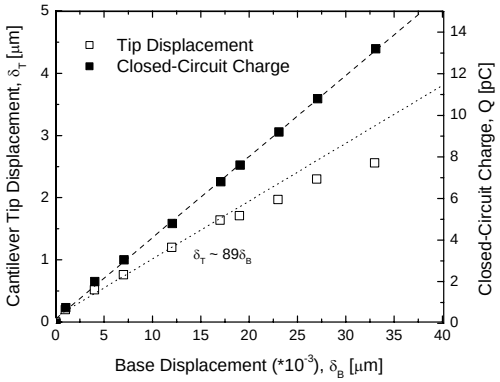

Figure 7. *Cantilever tip displacement and generated closed-circuit charge vs. base displacement.*

The amount of charge developed on the IDT electrode is approximately linear in proportion to tip displacement (In fact, the charge is more linear with the base displacement). This is because the axial stress developed within the PZT layer also increases linearly with tip displacement. A maximum generated charge of 13.2 pC was measured at a maximum tip displacement of 2.56 μm. The charge increases linearly with tip displacement with a linearity coefficient of 4.14 pC/μm.

For the next set of base shaking experiments, the PMPG device was connected to a bridge rectifying circuit with a resistive load across the storage capacitor, as shown in Fig. 5. The load voltage was measured as a function of load resistance with a fixed base displacement magnitude of 14 nm at a shaking frequency of 13.9 kHz. Figure 8 shows the load voltage and power delivered to the load. As expected, the load voltage increases with the increased load, up to 3 V at 10.1 MΩ. However, the power delivered to the load will not increase indefinitely. There is a maximum point, 1.01 μW for the 5.2 MΩ load, after which the electrical power decreases with increased load resistance. A 2.4V DC voltage was achieved at the 1.01 μW power level. Given the device area (including room for on-chip rectification and energy storage circuitry), this translates to an energy density of 0.74 mW-h/cm^2, which compares favorably to current chemical battery solutions (i.e. lithium ion). The storage capacitor charging and discharging times were approximately 0.2 and 0.3 seconds, respectively.

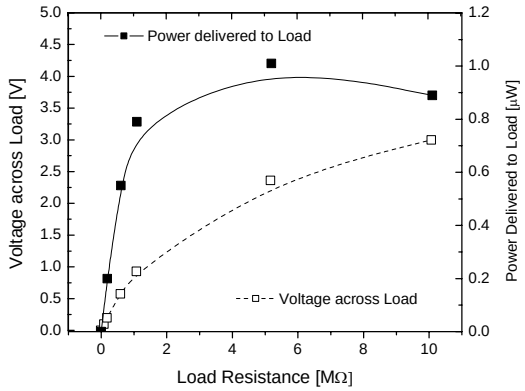

Figure 8. *Load voltage and power delivered to the load vs. load resistance at 13.9 kHz resonance.*

Going back to Eq. (3), the power is inversely proportional to the frequency and proportional to the square of the vibration amplitude. It is known that the amplitude of an ambient vibration source is inversely proportional to the square of its frequency; that is, $Y \sim 1/\omega_n^2$ [**1**]. Considering this property of the vibration source, the power decreases with frequency because the decreasing input base displacement amplitude dominates the increasing frequency contribution. This indicates that, in order to harness the most power from the available energy spectrum, the PMPG should target a lower frequency, perhaps in the few hundreds of Hz. From a conservative viewpoint, the power may not increase exactly linearly with decreasing frequency. Nevertheless, we should be able to achieve at least an order of magnitude more power by tuning the resonance frequency down to several hundred Hz.

However, there is one limitation in scaling down the frequency: The PZT material has a strain limit of approximately 10^{-3} to bear the vibration amplitude. Currently, the tip displacement of the PMPG for the 1.01 μW power generation is approximately 2 μm, roughly corresponding to a PZT strain of below 10^{-4} for the 170 μm long cantilever beam. Consequently, this lower frequency device has more capacity for getting a higher power output, but we have to compromise it within the PZT strain ability.

CONCLUSIONS

A MEMS-based d_{33} mode PMPG device was designed to have a high open-circuit voltage and power output while requiring only three photo masks for fabrication. Adjusting the residual stress and elastic modulus of the bottom membrane layer of the composite beam successfully controlled the bowing and resulted in a flat cantilever composite beam.

The cantilever has three different resonance modes: two bending (13.9 and 48.5 kHz) and one torsional (21.9 kHz). The packaged PMPG device was shaken by a piezoelectric shaker with a base displacement of 14 nm. A maximum DC voltage of 3V was generated across the load (10.1 MΩ), and a continuous electrical power of over 1μW was delivered to the 5.2 MΩ load. The corresponding energy density is 0.74 mW-h/cm^2, which compares favorably to current lithium ion chemical battery solutions. This d_{33} type, thin film, piezoelectric micro cantilever device could be used for various applications such as batteryless and wireless micro sensors and micro power generators. Targeting of the ambient power spectrum at lower frequencies could result in a higher power PMPG device in the future.

REFERENCES

1. S. Roundy, P. K. Wright, and J. Rabaey, "A Study of Low Level Vibrations as a Power Source for Wireless Sensor Nodes", *Computer Communications*, 26**,** 1131 (2003).
2. C. W. Wong, Y. Jeon, G. Barbastathis, and S-G. Kim, "Strain-Tuning of Periodic Optical Devices: Tunable Gratings and Photonic Crystals", *Technical Digest of the 2002 Solid-State Sensor and Actuator Workshop*, Hilton Head Isl., SC, 6/2-6/02, Transducer Research Foundation, Cleveland (2002), pp. 342-345.
3. K. Hwang, M. Koo, and S. Kim, "High-Brightness Projection Display Systems Based on the Thin-Film Actuated Mirror Array (TFAMA)", *Proc. of SPIE, Sep. 20-24*, 3513, *Santa Clara* (1998), pp. 171-180.
4. P. Glynne-Jones, S. P. Beeby and N. M. White, "Towards a Piezoelectric Vibration-Powered Microgenerator", *IEEE Proc.-Sci. Meas. Technol.*, 148, (2001), pp. 69-72.
5. J. Kymissis, C. Kendall, J. Paradiso and N. Gershenfeld, "Parasitic Power Harvesting in Shoes", *Proc. of the Second IEEE International Conference on Wearable Computing (ISWC)*, (1998), pp. 132-39
6. C. B. Williams and R. B. Yates, "Analysis of a Micro Electric Generator for Microsystems", *Proceedings of the Transducers 95/Eurosensor IX*, (1995), pp 369-372.
7. T. S. Low and W. Guo, "Modeling of a Three-Layer Piezoelectric Bimorph Beam With Hysteresis", *J. MEMS*, 4, 230 (1995).
8. J.F. Lynch, C.G. Ruderer and W.H. Duckworth, "Engineering Properties of Selected Ceramic Materials", *American Ceramic Society*, (1966), Based on report AFML-TR-66-52.
9. M. Fukuhara and A. Sanpei, "Effects on High-Temperature-Elastic properties on α-/β-Quartz Phase Transition of Fused Quartz", *J. Mater. Sci. Lett.*, 18, 751 (1999).
10. S. Sakaguchi, N. Murayama, Y. Kodama, and F. Wakai, "The Poissons Ratio of Engineering Ceramics at Elevated Temperature", *J. Mater. Sci. Lett.*, 10, 282 (1991).